

Empirical validation of models to compute solar irradiance on inclined surfaces for building energy simulation

P.G. Loutzenhiser^{1,2}, H. Manz¹, C. Felsmann³, P.A. Strachan⁴, G.M. Maxwell²

¹ Swiss Federal Laboratories for Materials Testing and Research (EMPA), Laboratory for Applied Physics in Buildings, CH-8600 Duebendorf, Switzerland

² Iowa State University, Department of Mechanical Engineering, Ames, IA 50011 USA

³ Technical University of Dresden, Institute of Thermodynamics and Building Systems Engineering, D-01062 Dresden, Germany

⁴ University of Strathclyde, Department of Mechanical Engineering, ESRU, Glasgow G1 1XJ, Scotland

Keywords: Solar radiation models; Empirical validation; Building energy simulation; Uncertainty analysis

Abstract

Accurately computing solar irradiance on external facades is a prerequisite for reliably predicting thermal behavior and cooling loads of buildings. Validation of radiation models and algorithms implemented in building energy simulation codes is an essential endeavor for evaluating solar gain models. Seven solar radiation models implemented in four building energy simulation codes were investigated: 1) isotropic sky, 2) Klucher 3) Hay-Davies, 4) Reindl, 5) Muneer, 6) 1987 Perez, and 7) 1990 Perez models. Solar radiation data from two 25 days period in October and March/April, which included diverse atmospheric conditions and solar altitudes, measured on the EMPA campus in a suburban area in Duebendorf, Switzerland, were used for validation purposes. Two of the three measured components of solar irradiances—global horizontal, diffuse horizontal and direct-normal—were used as inputs for calculating global irradiance on a south-west façade. Numerous statistical parameters were employed to analyze hourly measured and predicted global vertical irradiances. Mean absolute deviations for both periods were found to be: 1) 13.7% and 14.9% for the isotropic sky model, 2) 9.1% for the Hay-Davies model, 3) 9.4 % for the Reindl model, 4) 7.6% for the Muneer model, 5) 13.2% for the Klucher model, 6) 9.0%, 7.7%, 6.6%, and 7.1% for the 1990 Perez models, and 7) 7.9% for the 1987 Perez model. Detailed sensitivity analyses using Monte Carlo and Fitted Effects for N-way Factorial analyses were applied to assess how uncertainties in input parameters propagated through one of the building energy simulation codes and impacted the output parameter. The implications of deviations in computed solar irradiances on predicted thermal behavior and cooling load of buildings are discussed.

1. Introduction

In the 21st century, engineers and architects are relying increasingly on building energy simulation codes to design more energy-efficient buildings. One of the common traits found in new commercial buildings across Europe and the United States is construction with large glazed façades. Accurate modeling of the impact of solar gains through glazing is imperative especially when simulating the thermal behavior of these buildings. Empirical validations of solar gain models are therefore an important and necessary endeavor to provide confidence to developers and modelers that their respective algorithms simulate reality.

A preliminary step in assessing the performance of the solar gain models is to examine and empirically validate models that compute irradiance on exterior surfaces. Various radiation models for inclined surfaces have been proposed—some of which have been implemented in building energy simulation codes—which include isotropic models (Hottel and Woerz, 1942 as cited by Duffie and Beckman, 1991; Liu and Jordan 1960; Badescu, 2002), anisotropic models (Perez *et al.*, 1990, 1986; Gueymard, 1987; Robledo and Soler, 2002; Li *et al.*, 2002; Olmo *et al.*, 1999) and models for a clear sky (Robler and Soler, 2002). Comparisons and modifications to these models and their applications to specific regions in the world have also been undertaken (Behr, 1997; Ruiz *et al.*, 2002; Remund *et al.*, 1998).

Nomenclature

A	anisotropic index, -	i, j	indices the n-factorial study the represent different levels of input parameters
B	radiation distribution index, -	\overline{OU}	average overall uncertainty calculated for 95% credible limits, , W/m ²
a, b	terms that account for the incident angle on the sloped surface, -	s	sample standard deviation, W/m ²
D_{max}	maximum difference between experimental and predicted values for a given array, W/m ²	R_b	variable geometric factor which is a ratio of tilted and horizontal solar beam irradiance
D_{min}	minimum difference between experimental and predicted values for a given array, W/m ²	u	is the specific effects from the n-factorial study, W/m ²
D_{rms}	root mean squared difference between experimental and predicted values for a given array, W/m ²	TF	tilt factor, -
$D_{95\%}$	Ninety-fifth percentile of the differences between experimental and predicted values for a given array, W/m ²	UR	computed hourly uncertainty ratio for comparing overall performance of a given model
d	estimated error quantity provided by the manufacturer, units vary	\overline{UR}	average uncertainty ratio, -
F_1	circumsolar coefficient, -	UR_{max}	maximum uncertainty ratio, -
F_2	brightness coefficient, -	UR_{min}	minimum uncertainty ratio, -
F'	clearness index, -	\bar{x}	arithmetic mean for a given array of data, W/m ²
$f_{11}, f_{12}, f_{13}, f_{21}, f_{22}, f_{23}$	statistically derived coefficients derived from empirical data for specific locations as a function of ϵ_s , -	x_{min}	minimum quantity for a given array of data, W/m ²
I_{bn}	direct-normal solar irradiance, W/m ²	x_{max}	maximum quantity for a given array of data, W/m ²
I_h	global horizontal solar irradiance, W/m ²	Greek Symbols	
$I_{h,b}$	direct-normal component of solar irradiance on the horizontal surface, W/m ²	α	absorptance, %
$I_{h,d}$	global diffuse horizontal solar irradiance, W/m ²	α_n	normal absorptance, %
I_{on}	direct extraterrestrial normal irradiance, W/m ²	α_s	solar altitude angle, °
I_T	solar irradiance on the tilted surface, W/m ²	β	surface tilt angle from horizon, °
$I_{T,b}$	direct-normal (beam) component of solar irradiance on the tilted surface, W/m ²	Δ	sky condition parameter for brightness
$I_{T,d}$	diffuse component of solar irradiance on the tilted surface, W/m ²	ϵ	sky condition parameter for clearness
$I_{T,d,iso}$	isotropic diffuse component of solar irradiance on the tilted surface, W/m ²	ϕ_b	building azimuth, °
$I_{T,d,cs}$	circumsolar diffuse component of solar irradiance on the tilted surface, W/m ²	θ	incident angle of the surface, °
$I_{T,d,hb}$	horizontal brightening diffuse component of solar irradiance on the tilted surface, W/m ²	θ_z	zenith angle, °
$I_{T,d,g}$	reflected ground diffuse component of solar irradiance on the tilted surface, W/m ²	ξ	input parameter n-way factorial, units vary
		ρ	hemispherical-hemispherical ground reflectance, -
		σ	standard deviation n-way factorial, units vary

- 1 In all empirical validations, accounting for uncertainties in the experiment and input parameters is
- 2 paramount. Sensitivity analysis is a well-established technique in computer simulations (Saltelli *et al.* 2004,
- 3 2000; Santer *et al.*, 2003) and has been implemented in building energy simulation codes (Macdonald and

1 Strachan, 2001) and empirical validations (Mara *et al.*, 2001; Aude *et al.*, 2000; Fürbringer and Roulet, 1999,
2 1995; Lomas and Eppel, 1992) for many years. A thorough methodology for sensitivity analysis for
3 calculations, correlation analysis, principle component analysis, and implementation in the framework of
4 empirical validations in IEA-SHC Task 22 are described by Palomo Del Barrio and Guyon (2004; 2003).

5
6 In the context of the International Energy Agency's (IEA) SHC Task 34/ ECBCS Annex 43 Subtask C, a
7 series of empirical validations is being performed in a test cell to assess the accuracy of solar gain models in
8 building energy simulation codes with/without shading devices and frames. A thorough description of the
9 proposed suite of experiments, description of the cell, rigorous evaluation of the cell thermophysical
10 properties and thermal bridges, and a methodology for examining results are reported by Manz *et al.* (2005).

11
12 In virtually all building energy simulation applications, solar radiation must be calculated on tilted surfaces.
13 These calculations are driven by solar irradiation inputs or appropriate correction factors and clear sky
14 models. While the horizontal irradiation is virtually always measured, measuring of direct-normal and/or
15 diffuse irradiance adds an additional level of accuracy (Note: In the absence of the latter two parameters,
16 models have to be used to split global irradiation into direct and diffuse).

17
18 The purpose of this work is to validate seven solar radiation models on tilted surfaces that are implemented
19 in widely used building energy simulation codes including: EnergyPlus(2005), DOE-2.1e(2002), ESP-r
20 (2005), and TRNSYS-TUD (2005). The seven models examined include:

- 21 • Isotropic sky (Hottel and Woertz, 1942 as cited by Duffie and Beckman, 1991)
- 22 • Klucher (1979)
- 23 • Hay-Davies(1980)
- 24 • Reindl (1990)
- 25 • Muneer (1997)
- 26 • Perez (1987)
- 27 • Perez (1990)

28
29 Two of three measured irradiance components were used in each simulation and predictions of global
30 vertical irradiance on a façade oriented 29° West of South were compared with measurements. Particular
31 emphasis was placed on quantifying how uncertainty in the input parameters—direct-normal, diffuse and
32 horizontal global solar irradiance as well as ground reflectance and surface azimuth angle—propagated
33 through radiation calculation algorithms and impacted the global vertical irradiance calculation. Sensitivity
34 analyses were performed using both the Monte Carlo Analysis (MCA) and Fitted Effects for N-way
35 Factorials.

36 37 **2. Solar Radiation Models**

38 Total solar irradiance on a tilted surface can be divided into two components: 1) the beam component from
39 direct irradiation of the tilted surface and 2) the diffuse component. The sum of these components equates to
40 the total irradiance on the tilted surface and is described in Equation 1.

$$41 \quad I_T = I_{T,b} + I_{T,d} \quad [1]$$

42 Studies of clear skies have led to a description of the diffuse component being composed of an isotropic
43 diffuse component (uniform irradiance from the sky dome), circumsolar diffuse component (resulting from
44 the forward scattering of solar radiation and concentrated in an area close to the sun), horizon brightening
45 component (concentrated in a band near the horizon and most pronounced in clear skies), and a reflected
46 component that quantifies the radiation reflected from the ground to the tilted surface. A more complete
47 version of Equation 1 containing all diffuse components is given in Equation 2.

$$48 \quad I_T = I_{T,b} + I_{T,d,iso} + I_{T,d,cs} + I_{T,d,hb} + I_{T,d,g} \quad [2]$$

1 For a given location (longitude, latitude) at any given time of the year (date, time) the solar azimuth and
 2 altitude can be determined applying geometrical relationships. Therefore, the incidence angle of beam
 3 radiation on a tilted surface can be computed. The models described in this paper all handle beam radiation
 4 in this way so the major modeling differences are calculations of the diffuse radiation. An overview of solar
 5 radiation modeling used for thermal engineering is provided in numerous textbooks including Duffie and
 6 Beckman (1991) and Muneer (1997). Solar radiation models with different complexity which are widely
 7 implemented in building energy simulation codes will be briefly described in the following sections.

9 **2.1 Isotropic Sky Model**

10 The isotropic sky model (Hottel and Woertz, 1942 as cited by Duffie and Beckman, 1991; Liu and Jordan,
 11 1960) is the simplest model that assumes all diffuse radiation is uniformly distributed over the sky dome and
 12 that reflection on the ground is diffuse. For surfaces tilted by an angle β from the horizontal plane, total solar
 13 irradiance can be written as

$$14 \quad I_T = I_{h,b}R_b + I_{h,d}\left(\frac{1 + \cos \beta}{2}\right) + I_h\rho\left(\frac{1 - \cos \beta}{2}\right) \quad [3]$$

15 Circumsolar and horizon brightening parts (Eq. 2) are assumed to be zero.

17 **2.2 Klucher Model**

18 Klucher (1979) found that the isotropic model gave good results for overcast skies but underestimates
 19 irradiance under clear and partly overcast conditions, when there is increased intensity near the horizon and
 20 in the circumsolar region of the sky. The model developed by Klucher gives the total irradiation on a tilted
 21 plane shown in Equation 4.

$$22 \quad I_T = I_{h,b}R_b + I_{h,d}\left(\frac{1 + \cos \beta}{2}\right)\left[1 + F' \sin^3\left(\frac{\beta}{2}\right)\right]\left[1 + F' \cos^2 \vartheta \sin^3 \vartheta\right] + I_h\rho\left(\frac{1 - \cos \beta}{2}\right) \quad [4]$$

23 F' is a clearness index given by Equation 5.

$$24 \quad F' = 1 - \left(\frac{I_{h,d}}{I_h}\right)^2 \quad [5]$$

25 The first of the modifying factors in the sky diffuse component takes into account horizon brightening; the
 26 second takes into account the effect of circumsolar radiation. Under overcast skies, the clearness index F'
 27 becomes zero and the model reduces to the isotropic model.

29 **2.3 Hay-Davies Model**

30 In the Hay-Davies model, diffuse radiation from the sky is composed of an isotropic and circumsolar
 31 component (Hay and Davies, 1980) and horizon brightening is not taken into account. The anisotropy index
 32 A defined in Equation 6 represents the transmittance through atmosphere for beam radiation.

$$33 \quad A = \frac{I_{bn}}{I_{on}} \quad [6]$$

34 The anisotropy index is used to quantify a portion of the diffuse radiation treated as circumsolar with the
 35 remaining portion of diffuse radiation assumed isotropic. The circumsolar component is assumed to be from
 36 the sun's position. The total irradiance is then computed in Equation 7.

$$37 \quad I_T = (I_{h,b} + I_{h,d}A)R_b + I_{h,d}(1 - A)\left(\frac{1 + \cos \beta}{2}\right) + I_h\rho\left(\frac{1 - \cos \beta}{2}\right) \quad [7]$$

38 Reflection from the ground is dealt with as for the isotropic model.

40 **2.4 Reindl Model**

41 In addition to isotropic diffuse and circumsolar radiation, the Reindl model also accounts for horizon
 42 brightening (Reindl *et al*, 1990a; Reindl *et al*, 1990b) and employs the same definition of the anisotropy

1 index A as described in Equation 6. The total irradiance on a tilted surface can then be calculated using
2 Equation 8.

$$3 \quad I_T = (I_{h,b} + I_{h,d}A)R_b + I_{h,d}(1-A)\left(\frac{1+\cos\beta}{2}\right)\left[1 + \sqrt{\frac{I_{h,b}}{I_h}} \sin^3\left(\frac{\beta}{2}\right)\right] + I_h\rho\left(\frac{1-\cos\beta}{2}\right) \quad [8]$$

4 Reflection on the ground is again dealt with as for the isotropic model. Due to the additional term in
5 Equation 8 representing horizon brightening, the Reindl model provides slightly higher diffuse irradiances
6 than the Hay-Davies model.

7 **2.5 Muneer Model**

9 Muneer's model is summarized by Muneer (1997). In this model the shaded and sunlit surfaces are treated
10 separately, as are overcast and non-overcast conditions of the sunlit surface. A tilt factor T_F representing the
11 ratio of the slope background diffuse irradiance to the horizontal diffuse irradiance is calculated from
12 Equation 9.

$$13 \quad T_F = \left(\frac{1+\cos\beta}{2}\right) + \frac{2B}{\pi(3+2B)}\left[\sin\beta - \beta\cos\beta - \pi\sin^2\frac{\beta}{2}\right] \quad [9]$$

14 For surfaces in shade and sunlit surfaces under overcast sky conditions, the total radiation on a tilted plane is
15 given in Equation 10.

$$16 \quad I_T = I_{h,b}R_b + I_{h,d}T_F + I_h\rho\left(\frac{1-\cos\beta}{2}\right) \quad [10]$$

17 Sunlit surfaces under non-overcast sky conditions can be calculated using Equation 11.

$$18 \quad I_T = I_{h,b}R_b + I_{h,d}[T_F(1-A) + AR_b] + I_h\rho\left(\frac{1-\cos\beta}{2}\right) \quad [11]$$

19 The values of the radiation distribution index B depend on the particular sky and azimuthal conditions, and
20 the location. For European locations, Muneer recommends fixed values for the cases of shaded surfaces and
21 sun-facing surfaces under an overcast sky, and a function of the anisotropic index for non-overcast skies.

22 **2.6 Perez Model**

24 Compared with the other models described, the Perez model is more computationally intensive and
25 represents a more detailed analysis of the isotropic diffuse, circumsolar and horizon brightening radiation by
26 using empirically derived coefficients (Perez *et al.*, 1990). The total irradiance on a tilted surface is given by
27 Equation 12.

$$28 \quad I_T = I_{h,b}R_b + I_{h,d}\left[(1-F_1)\left(\frac{1+\cos\beta}{2}\right) + F_1\frac{a}{b} + F_2\sin\beta\right] + I_h\rho\left(\frac{1-\cos\beta}{2}\right) \quad [12]$$

29 Here, F_1 and F_2 are circumsolar and horizon brightness coefficients, respectively, and a and b are terms that
30 take the incidence angle of the sun on the considered slope into account. The terms a and b are computed
31 using Equations 13 and 14, respectively.

$$32 \quad a = \max(0, \cos\theta) \quad [13]$$

$$33 \quad b = \max(\cos 85, \cos\theta_z) \quad [14]$$

34 The brightness coefficients F_1 and F_2 depend on the sky condition parameters clearness ε and brightness Δ .
35 These factors are defined in Equations 15 and 16, respectively.

$$36 \quad \varepsilon = \frac{\frac{I_{h,d} + I_n}{I_{h,d}} + 5.535 \cdot 10^{-6} \theta_z^3}{1 + 5.535 \cdot 10^{-6} \theta_z^3} \quad [15]$$

$$37 \quad \Delta = m \frac{I_{h,d}}{I_{on}} \quad [16]$$

1 F_1 and F_2 are then computed in Equations 17 and 18, respectively.

$$2 \quad F_1 = \max \left[0, \left(f_{11} + f_{12} \Delta + \frac{\pi \theta_z}{180} f_{13} \right) \right] \quad [17]$$

$$3 \quad F_2 = f_{21} + f_{22} \Delta + \frac{\pi \theta_z}{180} f_{23} \quad [18]$$

4 The coefficient f_{11} , f_{12} , f_{13} , f_{21} , f_{22} , and f_{23} were derived based on a statistical analysis of empirical data for
5 specific locations. Two different sets of coefficients were derived for this model (Perez *et al.*, 1990; 1988 as
6 cited by Duffie and Beckman, 1991). An earlier version of the model with different coefficients (Perez
7 1987) was also included in this analysis.

8

9 **3. Facility and Measurements**

10 **3.1 Test Site and Setup**

11 The solar radiation measurements were performed on the EMPA campus located in Duebendorf, Switzerland
12 (Longitude 8°36'55", Latitude 47°24'12"). Figure 1 shows the facility which was designed to measure solar
13 gains of transparent façade components; a detailed description of facility is provided by Manz *et al.* (2005).
14 For this study, only the pyranometers and the pyrliometer at the facility were used (Figures 1 and 2). For
15 the diffuse measurements, a shading disk was mounted in front of the pyranometer with the same solid angle
16 as the pyrliometer that blocked out the beam irradiance component (Figure 2). In order to evaluate the
17 robustness of various radiation models, two 25 day periods were studied to compare predicted irradiance on
18 the tilted façade with measured data that were recorded by a pyranometer mounted on the vertical surface
19 (29° West of South) of the test cell. The dates of the first and second periods were October 2 to October 26,
20 2004 and March 22 to April 16, 2005, respectively. Both periods include a range of different atmospheric
21 conditions and solar positions. The solar radiation data were acquired for 600 h for each period.

22

23 **3.2 Solar Irradiance**

24 Table 1 indicates measured parameters, type of instrument used and accuracies of sensors specified by the
25 manufacturers. To verify the accuracy of the instrumentation, the global horizontal irradiance can be
26 calculated using solar position and direct-normal and horizontal diffuse irradiance shown in Equation 19.

$$27 \quad I_h = I_{b,n} \sin \alpha_s + I_{h,d} \quad [19]$$

28 The differences between global horizontal irradiance measured and computed based on direct-normal (beam)
29 and horizontal diffuse irradiance were analyzed. Using the experimental uncertainties described in Table 1,
30 95% credible limits were calculated for the measured global horizontal irradiance using manufacturer's error
31 and for the computed global irradiance using propagation of error techniques (uncertainty analysis) assuming
32 uniform distributions (Glesner, 1998). From these comparisons, the 95% credible limits from the calculated
33 and measured global horizontal irradiance for Periods 1 and 2 were found to overlap 78.0% and 70.1% of the
34 time, respectively; these calculations were only performed when the sun was up ($\alpha_s > 0$). Careful
35 examination of these results reveals that the discrepancies occurred when the solar altitude angles and
36 irradiance were small or the solar irradiance were very large (especially for Period 2). Linear regression
37 analysis was used to compare the computed and measured global irradiances. The results from this analysis
38 are shown for Periods 1 and 2 in Figures 3a and 3b, respectively. The differences between calculated and
39 measured quantities are apparent from the slopes of lines. These results reveal a slight systematic under-
40 prediction by roughly 3% of global horizontal irradiance when calculating it from the beam and diffuse
41 horizontal irradiance components.

42

43 **3.3 Ground Reflectance**

44 The importance of accurately quantifying the albedo in lieu of relying on default values is discussed in detail
45 by Ineichen *et al.* (1987). Therefore, in order to have a well-defined and uniform ground reflectance,
46 artificial green turf was installed in front of the test cell to represent a typical outdoor surface (Figure 1).

47

1 Reflectance of a sample of the artificial turf was measured at almost perpendicular (3°) incident radiation in
 2 the wavelength interval between 250 nm and 2500 nm using an integrating sphere (Figure 4) which could not
 3 be employed for angular dependent measurements. Specular components of the reflectance were measured at
 4 incident angles of 20° , 40° , and 60° and were found to be less than 1%; therefore the surface was considered
 5 to be a Lambertian surface (Modest, 2003). Integral values for reflectance were determined according to EN
 6 410 (1998) by means of GLAD software (2002). Hemispherical-hemispherical reflectance was then
 7 determined at each wavelength assuming an angular dependent surface absorptance as shown in Equation 20
 8 (from Duffie and Beckman, 1991).

$$\frac{\alpha(\theta)}{\alpha_n} = \begin{cases} 1 + 2.0345 \times 10^{-3} \theta - 1.99 \times 10^{-4} \theta^2 + 5.324 \times 10^{-6} \theta^3 - 4.799 \times 10^{-8} \theta^4 & 0^\circ \leq \theta \leq 80^\circ \\ -0.064\theta + 5.76 & 80^\circ \leq \theta \leq 90^\circ \end{cases} \quad [20]$$

11 Equation 21 was used to calculate the hemispherical-hemispherical reflectance.

$$\rho = 2 \int_{0^\circ}^{90^\circ} (1 - \alpha(\theta)) \sin(\theta) \cos(\theta) d\theta \quad [21]$$

13 This integral was evaluated numerically using the Engineering Equation Solver (Klein, 2004). The computed
 14 solar ground reflectance (Table 2) corresponds well with albedo measurements described by Ineichen *et al.*
 15 (1987).

17 4. Simulations

18 The incident (global vertical) irradiance on the exterior façade for all the building energy simulation codes
 19 was a function of the solar irradiance and ground reflectance. Four building energy simulation codes,
 20 EnergyPlus, DOE-2.1e, ESP-r and TRNSYS-TUD, which included seven different radiation models were
 21 evaluated for both periods.

23 EnergyPlus version 1.2.2 uses the 1990 Perez model. For the simulation, measured direct-normal and diffuse
 24 horizontal solar irradiance were used as inputs in 10 minute time steps. DOE-2.1e also uses a Perez 1990
 25 model to calculate irradiance on a tilted façade (Buehl, 2005) with hourly inputs of direct-normal and global
 26 horizontal solar irradiance. Both EnergyPlus and DOE-2.1e assumed a constant annual direct-normal
 27 extraterrestrial irradiation term (they do not factor in the elliptical orbit of the earth around the sun).
 28 TRNSYS-TUD allows the user to select from four models and various inputs for solar irradiance. For these
 29 experiments, the Isotropic, Hay-Davies, Reindl, and Perez 1990 model were used with inputs of measured
 30 direct normal and global horizontal irradiance; the inputs to the models were in 1 hour time steps. An
 31 average annual extraterrestrial irradiation term was also assumed for the Perez, Reindl, and Hay-Davies
 32 models. ESP-r has the Perez 1990 model as its default, but other models are available to the user, namely the
 33 Isotropic, Klucher, Muneer and Perez 1987 models. Measured 6 minutely averaged data were input to the
 34 program. The program takes into account variations in the extraterrestrial radiation in the Perez and Muneer
 35 models. It is also possible to use direct normal plus diffuse horizontal irradiation, or global horizontal plus
 36 diffuse horizontal irradiation as inputs to ESP-r; for this study, only the direct normal and diffuse horizontal
 37 inputs were studied.

39 5. Sensitivity Analysis

40 Sensitivity studies are an important component in thorough empirical validations; such studies were therefore
 41 also performed. The uncertainties in the input parameters were taken from information provided by the
 42 manufacturers (Table 1). The error in the ground reflectance calculation (models and measurements
 43 combined) was estimated as 5% (see Table 2) and $\pm 1^\circ$ for the building azimuth. Uniform distributions were
 44 assumed for estimated uncertainties and quantities provided by manufacturers (Glesner, 1998). Although all
 45 the codes perform solar angle calculations, uncertainties were not assigned to the cell locations (latitude and
 46 longitude). Two types of sensitivity analysis were performed for this project in EnergyPlus which included
 47 Fitted Effects for N-way Factorials and MCA. For these analyses the source code was not modified, but

1 rather a “wrap” was designed to modify input parameters in the weather file and the input file for EnergyPlus
 2 in MatLab 7.0 (2004). A Visual Basic program was written to create a command line executable program to
 3 run the “WeatherConverter” program and the “RunEplus.bat” program was run from the MatLab programs.
 4 Output from each run was recorded in output files. A flowchart for this process is depicted in Figure 6.

6 **5.1. Fitted Effects for N-way Factorials**

7 A Fitted Effects N-way Factorial method was used to identify the impact of uncertainties in various
 8 parameters on the results (Vardeman and Jobe, 2001). The parameters that were varied for this study
 9 included: ground reflectance, direct-normal irradiance, global horizontal irradiance (which was an unused
 10 parameter in EnergyPlus), and diffuse irradiance. Therefore, for this study a fitted effects for a three-way
 11 factorial analysis was performed. The first step in this process is to run a one-way factorial shown in
 12 Equation 22 varying each parameter.

$$13 \quad u_i = \phi(\xi_i + \sigma_i) - \phi(\xi_i) \quad [22]$$

14 For uniform distributions, the standard deviation is estimated in Equation 23.

$$15 \quad \sigma_i = \frac{d}{\sqrt{3}} \quad [23]$$

16 The two-way factorials were estimated using Equation 24. Additional levels of interactions were considered
 17 but were found to be negligible.

$$18 \quad u_{ij} = \phi(\xi_i + \sigma_i, \xi_j + \sigma_j) - (\phi(\xi_i, \xi_j) + u_i + u_j) \quad i \neq j \quad [24]$$

19 The overall uncertainty was estimated using the quadrature summation shown in Equation 25.

$$20 \quad u = \sqrt{\sum u_i^2 + \sum u_{ij}^2} \quad [25]$$

21 This analysis assumes a localized linear relationship where the function is evaluated. To confirm this
 22 assumption, estimates were made by forward differencing ($\xi_i + \sigma_i$) and backward differencing ($\xi_i - \sigma_i$). The
 23 individual factorials can also be analyzed to assess their impact. In Table 3, the results from this analysis
 24 averaged over the entire test ($\alpha_s > 0$) are shown for both forward and backward differencing. Looking at the
 25 results from forward and backward difference, the assumed localized linear relationship seems reasonable
 26 but may lead to minor discrepancies that are discussed later.

28 **5.2. Monte Carlo Analysis**

29 The Monte Carlo method can be used to analyze the impact of all uncertainties simultaneously by randomly
 30 varying input parameters and performing multiple evaluations of the output parameter(s). When setting up
 31 the analysis, the inputs are modified according to a probability density function (pdf) and, after numerous
 32 iterations, the outputs are assumed to be Gaussian (normal) by the Central Limit Theorem. The error is
 33 estimated by taking the standard deviation of the multiple evaluations at each time step. MatLab 7.0 can be
 34 used to generate random numbers according to Gaussian, uniform, and many other distributions. A
 35 comprehensive description and the underlying theory behind the Monte Carlo Method are provided by
 36 Fishman (1996) and Rubinstein (1981).

38 **5.2.1. Sampling**

39 For this study, Latin hypercube sampling was used. In this method, the range of each input factor is divided
 40 into equal probability intervals based on the number of runs of the simulation; one value is then taken from
 41 each interval. When applying this method for this study given parameters with non-uniform distributions,
 42 the intervals were defined using the cumulative distribution function and then one value was selected from
 43 each interval assuming a uniform distribution (again this was simplified in using MatLab because the
 44 functions were part of the code). This method of sampling is better when a few components of input
 45 dominate the output (Saltelli *et al.*, 2000). For this study, the input parameters were all sampled from a
 46 uniform distribution. Previous studies have shown that after 60-80 there are only slight gains in accuracy
 47 (Fürbringer and Roulet, 1995), but 120 runs were used to determine uncertainty. The average overall
 48 uncertainties ($\alpha_s > 0$) for Periods 1 and 2 were 2.35 W/m² and 2.87 W/m², respectively; the results

1 corresponded well with the fitted effects models. The results at any given time step are discussed in the next
2 section.

3 4 **5.2.2. Analysis of Output**

5 It can be shown that despite the pdf's for input parameters, the output parameters will always have a
6 Gaussian distribution (given a large enough sample and sufficient number of inputs) by the Central Limit
7 Theorem; therefore a Lilliefors Test for goodness of fit to normal distribution was used to test significance at
8 5% (when $\alpha_s > 0$). Using this criterion, 27.5% and 11.5% of the outputs from Periods 1 and 2, respectively,
9 were found not to be normally distributed. A careful study of these results reveals that the majority (not all)
10 of these discrepancies occurred when the direct-normal irradiance is small or zero. This may be due to the
11 proportional nature of the uncertainties used for these calculations. At low direct-normal irradiances, the
12 calculation becomes a function of only two inputs rather than three, which could make the pdf for the output
13 parameter more susceptible to the individual pdf's of the input parameters, which for these cases were
14 uniform distributions.

15 16 **5.3 Estimated Uncertainties**

17 Estimates for uncertainties were obtained from both Fitted Effects for N-way Factorial and MCA. From
18 these analyses, both methods yield similar results. The only discrepancies for both forward and backward
19 differencing were that fitted effects estimates are sometimes overestimated at several individual time steps.
20 Careful inspection of the individual responses revealed that there was a significant jump in the two-way
21 direct-normal/diffuse response (sometimes in the order of 5 W/m²) that corresponds to odd behavior in the
22 one-way responses. The response for the rest of the time steps was negligible. Additional review showed
23 that these events do not occur during the same time steps for forward and backward differencing. It was
24 therefore assumed that these discrepancies result from localized non-linearities at these time steps.

25 26 **6. Results**

27 The computed results from the four simulation codes were compared with the measured global vertical
28 irradiance. Comparisons were made using the nomenclature and methodology proposed by Manz *et al.*
29 (2005). An important term used for comparing the performance of the respective models in the codes is the
30 uncertainty ratio. This term was computed at each hour ($\alpha_s > 0$) and is shown in Equation 26. The average,
31 maximum, and minimum quantities are summarized in the statistical analyses for each test. Ninety-five
32 percent credible limits were calculated from the MCA for EnergyPlus and the 95% credible limits for the
33 experiment were estimated assuming a uniform distribution. The credible limits from EnergyPlus were used
34 to calculate the uncertainty ratios for all the models and codes. For the uncertainty ratio, terms less than
35 unity indicate that the codes are validated with 95% credible limits.

$$36 \quad UR = \frac{|D|}{OU_{Experiment} + OU_{EnergyPlus}} \quad [26]$$

37 Tables 4, 5, and 6 show the results from Periods 1 and 2 and combined periods, respectively. Plots were
38 constructed that depict the global vertical irradiation (hourly averaged irradiance values multiplied by a 1 hr
39 interval) and credible limits. For these plots, the output and 95% credible limits for a given hour of the day
40 were averaged to provide an overview of the performance of each model. Figures 6 to 8 contain results from
41 Periods 1 and 2 and the combined results.

42 43 **7. Discussion and Conclusions**

44 The accuracy of the individual radiation models and their implementation in each building energy simulation
45 code for both periods can be accurately assessed from the statistical analyses and the plots from the results
46 section. Figure 6 shows that in the morning, there are both over or under-prediction of the global vertical
47 irradiance by the models for Period 1; in the afternoon the global vertical irradiance are significantly under-
48 predicted. During Period 2, over-predictions from the statistical analysis can be seen in both the morning
49 and the afternoon from Figure 7, which explains results from the statistical analysis. Combining these results

1 helps to redistribute the hourly over and under-predictions from each model, but it is still clear all the models
2 performed better during Period 1.

3
4 Using the average uncertainty ratio as a guide, it can be seen that for both periods none of the models were
5 within overlapping 95% credible limits. Strictly speaking, none of the models can therefore be considered to
6 be validated within the defined credible limits ($\overline{UR} > 1$). This is partly due to the proportional nature of the
7 error which at vertical irradiance predictions with small uncertainties lead to large hourly uncertainty ratio
8 calculations and the difficulty in deriving a generic radiation model for every location in the world. This is
9 also shown in Figures 6 to 8 where there is very little overlap in the experimental and MCA 95% credible
10 limits. But the average uncertainty ratio can also be used as a guide to rank the overall performance of the
11 tilted radiation models. The Isotropic model performed the worst during these experiments, which can be
12 expected because it was the most simplistic and did not account for the various individual components of
13 diffuse irradiance. While the Reindl and Hay-Davies model accounted for the additional components of
14 diffuse irradiance (both circumsolar and horizontal brightening for the Reindl and circumsolar for the Hay-
15 Davies), the Perez formulation—which relied on empirical data to quantify the diffuse components—
16 provided the best results for this location and wall orientation. Differences between the Perez models in the
17 four building energy simulation codes can be attributed to solar irradiance input parameters (beam, global
18 horizontal, and diffuse), time steps of the weather measurements, solar angle algorithms, and assumptions
19 made by the programmers (constant direct-normal extraterrestrial radiations for DOE-2.1e and EnergyPlus).
20 For both periods, the assumptions made in the TRNSYS-TUD formulation Perez radiation model performed
21 best. But also from these results, the Muneer model performed quite well without the detail used in the Perez
22 models. In fact, the Muneer model performed better than Perez models formulated in EnergyPlus and DOE-
23 2.1e.

24
25 The presented results reveal distinct difference between radiation models that will ultimately manifest
26 themselves in the solar gain calculations. Mean absolute deviations in predicting solar irradiance for both
27 time periods were: 1) 13.7% and 14.9% for the isotropic sky model, 2) 9.1% for the Hay-Davies, 3) 9.4%
28 for the Reindl, 4) 7.6% for the Muneer model, 5) 13.2% for the Klucher, 6) 9.0%, 7.7%, 6.6%, and 7.1% for
29 the 1990 Perez, and 7) 7.9% for the 1987 Perez models. This parameter is a good estimate of the
30 instantaneous error that would impact peak load calculations. The mean deviations calculations for these
31 time periods were: 1) -5.3% and -7.7% for the isotropic sky model, 2) -1.1% for the Hay-Davies, 3) 2.6%
32 for the Reindl, 4) 2.8% for the Muneer model, 5) -6.2% for the Klucher, 6) 2.6%, 5.0%, 0.5%, and 1.0% for
33 the 1990 Perez, and 7) 3.5% for the 1987 Perez models. From this parameter it can be concluded that
34 building energy simulation codes with advanced radiation models are capable of computing total irradiated
35 solar energy on building façades with a high precision for longer time periods (such as months). Hence, the
36 calculations of building energy consumption with very high prediction accuracy is achievable even in
37 today's highly glazed buildings, which are largely affected by solar gains. On the other hand, even the most
38 advanced models deviate significantly at specific hourly time steps (up to roughly 100 W/m²), which poses
39 serious limitations to accuracy of predictions of cooling power at a specific point in time, the short-time
40 temperature fluctuations in the case of non-air conditioned buildings or the control and/or sizing of HVAC
41 equipment or shading devices. When performing building simulations, engineers must consider much higher
42 uncertainties at specific time steps.

43
44 Additional factors that were not investigated include the number of components of solar irradiance measured
45 at a given weather station (often only global horizontal irradiance is measured and other models are used to
46 compute beam irradiance), locations and densities of the weather stations used as inputs for building
47 simulation codes, and reliability of weather files used by building energy simulation codes.

48
49 Note: Radiation data and data of all other experiments within the IEA Task 34 project can be downloaded
50 from our website at www.empa.ch/ieatask34.

1 Acknowledgements

2 We gratefully acknowledge with thanks the financial support from the Swiss Federal Office of Energy (BFE)
3 for building and testing the experimental facility (Project 17'166) as well as the funding for EMPA
4 participation in IEA Task 34/43 (Project 100'765). We would also like to acknowledge Dr. M. Morris from
5 the Iowa State University Statistics Department for his clear direction with regard to formulating the
6 sensitivity analysis and the many contributions from our colleagues R. Blessing, S. Carl, M. Camenzind, T.
7 Frank and R. Vonbank.

11 References

- 12 Aude, P., Tabary, L., and Depecker, P., 2000. Sensitivity analysis and validation of buildings' thermal
13 models using adjoint-code method. *Energy and Buildings* 30:267-283
- 14 Badescu, V., 2002. 3D Isotropic approximation for solar diffuse irradiance on tilted surfaces. *Renewable*
15 *Energy* 26:221-233
- 16 Behr, H.D., 1997. Solar radiation on tilted south oriented surfaces: validation of transfer-models. *Solar*
17 *Energy* Vol. 61 No.6:399-413
- 18 Buehl, F., 2005. Private email correspondence exchanged on March 9, 2005 with Peter Loutzenhiser at
19 EMPA that contained the radiation model portion of the DOE-2.1E source code, LBNL
- 20 DOE-2.1E (Version-119). 2002. Building Energy Simulation Code, Lawrence Berkley Laboratories (LBL),
21 Berkley, CA, April 9, 2002
- 22 Duffie, J.A., and Beckman, W.A., 1991. *Solar Engineering of Thermal Processes 2nd Edition*, John Wiley &
23 Sons, New York, Chichester, Brisbane, Toronto, Singapore
- 24 EnergyPlus Version 1.2.2.030. 2005. Building Energy simulation code, www.energyplus.gov
25 ESP-r, Version 10.12, 2005, University of Strathclyde, www.esru.strath.ac.uk.
- 26 European Standard EN 410, 1998. Glass in building – Determination of luminous and solar characteristics of
27 glazing. European Committee for Standardization, Brussels, Belgium
- 28 Fishman, G.S., 2000. *Monte Carlo: Concepts, Algorithms, and Applications*, Springer, New York, Berlin,
29 Heidelberg
- 30 Fürbringer, J.M., and Roulet, C.A., 1999. Confidence of simulation results: put a sensitivity analysis module
31 in you MODEL: The IEA-ECBCS Annex 23 experience of model evaluation. *Energy and Buildings*
32 30:61-71
- 33 Fürbringer, J.M., and Roulet, C.A., 1995, Comparison and Combination of Factorial and Monte-Carlo
34 Design in Sensitivity Analysis. *Building and Environment* Vol. 30 No.4:505-519
- 35 Hay, J.E., Davies, J.A., 1980. Calculations of the solar radiation incident on an inclined surface, Proc. of
36 First Canadian Solar Radiation Data Workshop (Eds: J.E. Hay and T.K. Won), Ministry of Supply and
37 Services Canada, 59
- 38 Hottel, H.C. and Woetrz, B.B., 1942, Evaluation of flat-plate solar heat collector. *Trans. ASME* 64, 91
- 39 Ineichen, P., Perez, R., and Seals, R., 1987. The importance of correct albedo determination for adequately
40 modeling energy received by a tilted surface. *Solar Energy* Vol.39 No.4:301-305
- 41 GLAD Software, 2002. EMPA Material Science and Technology, Duebendorf, Switzerland
- 42 Glesner, J.L., 1998. Assessing Uncertainty in Measurement. *Statistical Science* Vol. 13 No.3:277-290
- 43 Gueymard, C., 1987. An anisotropic solar irradiance model for tilted surfaces and its comparison with
44 selected engineering algorithms. *Solar Energy* Vol.38 No.5:367-386
- 45 Klein, S.A., 2004. Engineering Equation Solver (EES) Software, Department of Mechanical Engineering,
46 University of Wisconsin—Madison
- 47 Klucher, T.M, 1979. Evaluation of models to predict insolation on tilted surfaces. *Solar Energy* 4,14.
- 48 Li, D.H.W., Lam, J.C., Lau, and Chris C.S., 2002. A new approach for predicting vertical global solar
49 irradiance. *Renewable Energy* 25:591-606

- 1 Lomas, K.J. and Eppel, H., 1992. Sensivity analysis techniques for building thermal simulation programs.
2 *Energy and Buildings* 19:21-44
- 3 Macdonald, I. and Strachan, P., 2001. Practical applications of uncertainty analysis. *Energy and Buildings*,
4 33:219-227
- 5 Mara, T.A., Garde, F., Boyer, H., and Mamode, M., 2001. Empirical validation of the thermal model of a
6 passive solar test cell. *Energy and Buildings* 33:589-599
- 7 MATLAB Version 7.0.0.19920, 2004. The MathWorks Inc.
- 8 Manz, H., Loutzenhiser, P., Frank, T., Strachan, P.A., Bundi, R., and Maxwell, G. (Submitted February 2005
9 to *Building and Environment*) Series of experiments for empirical validation of solar gain modeling in
10 building energy simulation codes – Experimental setup, test cell characterization, specifications and
11 uncertainty analysis.
- 12 Modest, M., 2003. *Radiative Heat Transfer 2nd Edition*, Academic Press, Amsterdam.
- 13 Muneer, T., 1997. Solar radiation and daylight models for the energy efficient design of buildings,
14 Architectural Press, Oxford.
- 15 Olmo, F.J., Vida, J., Castro-Diez, Y., and Alados-Arboledas, L., 1999. Prediction of global irradiance on
16 inclined surfaces from horizontal global irradiance. *Energy* 24:689-704
- 17 Palomo del Barrio, E., and Guyon, G., 2004. Application of parameters space analysis tools fro empirical
18 model validation. *Energy and Buildings* 36:23-33
- 19 Palomo del Barrio, E., and Guyon, G., 2003. Theoretical basis for empirical model validation using parameter
20 space analysis tools. *Energy and Buildings* 35:985-996
- 21 Perez, R., Stewart, R., Arbogast, C., Seals, R., and Scott, J., 1986. An anisotropic hourly diffuse radiation
22 model for sloping surfaces: Description, performance validation, site dependency evaluation. *Solar*
23 *Energy* Vol.36 No.6:481-497
- 24 Perez, R., Seals, R., Ineichen, P., Stewart, R., and Menicucci D., 1987. A new simplified version of the Perez
25 diffuse irradiance model for tilted surfaces. *Solar Energy* Vol.39 No.3:221-232
- 26 Perez, R., Stewart r., Seals, R., and Guertin, T. 1988. The development and verification of the Perez diffuse
27 radiation model. Sandia National Laboratories Contractor Report SAND88-7030
- 28 Perez, R., Ineichen, P., Seals, R., Michalsky, J., and Stewart, R., 1990. Modeling daylight availability and
29 irradiance components from direct and global irradiance. *Solar Energy* Vol.44 No.5:271-289
- 30 Reindl, D.T., Beckmann, W.A., Duffie, J.A., 1990a. Diffuse fraction correlations. *Solar Energy* 45:1-7
- 31 Reindl, D.T., Beckmann, W.A., Duffie, J.A., 1990b. Evaluation of hourly tilted surface radiation models.
32 *Solar Energy* 45:9-17
- 33 Remund, J., Salvisberg, E., and Kunz, S., 1998. On the generation of hourly shortwave radiation data on tilted
34 surfaces. *Solar Energy* Vol.62 No.5:331-334
- 35 Robledo, L. and Solar, A., 2002. A simple clear skies model for the luminous efficacy of diffuse solar
36 radiation on inclined surfaces. *Renewable Energy* 26:169-176
- 37 Rubinstein, R.Y., 1981. *Simulation and the Monte Carlo Method*, John Wiley & Sons, New York, Chichester,
38 Brisbane, Toronto
- 39 Saltelli, A., Tarantola, S., Campolongo, F., and Ratto, M., 2004. *Sensitivity Analysis in Practice: A Guide to*
40 *Assessing Scientific Models*, John Wiley & Sons, LTD
- 41 Saltelli, A., Chan, K., and Scott, E.M., 2000. *Sensitivity Analysis*, John Wiley & Sons, LTD, Chichester, New
42 York, Weinheim, Brisbane, Singapore, Toronto
- 43 Santner, T.J., Williams, B.J., and Notz, W.I., 2003. *The Design and Analysis of Computer Experiments*,
44 Springer, New York, Berlin, Heidelberg
- 45 TRNSYS-TUD, 2005, Technical University of Dresden research code based on the frame of TRNSYS 14.2,
46 Solar Energy Laboratory, University of Wisconsin-Madison, Madison, WI, 1996
- 47 Vardeman, S.B., and Jobe, J.M., 2001. *Data Collection and Analysis*, Duxbury Thomson Learning,
48 Australia, Canada, Mexico, Singapore, Spain, United Kingdom, United States
- 49

Table 1 Instruments used for measuring solar irradiance.

Parameter	Unit	Type of sensor / measurement	Number of sensors	Accuracy
Solar global irradiance, façade plane (29° W of S)	W/m ²	Pyranometer (Kipp & Zonen CM 21)	1	± 2 %
Solar global horizontal irradiance	W/m ²	Pyranometer (Kipp & Zonen CM 21)	1	± 2 %
Solar diffuse horizontal irradiance	W/m ²	Pyranometer, mounted under the shading ball of a tracker (Kipp & Zonen CM 11)	1	± 3 %
Direct-normal irradiance	W/m ²	Pyrheliometer, mounted in an automatic sun-following tracker(Kipp & Zonen CH 1)	1	± 2 %

Table 2 Solar ground reflectance.

Parameter	Reflectance, %
Hemispherical-Hemispherical	14.8 ± 0.74
Near Direct Normal-Hemispherical	8.8

Table 3 Average factorial impacts ($\alpha_S > 0$).

Factorial	Period 1		Period 2	
	Forward Differencing, W/m ²	Backward Differencing, W/m ²	Forward Differencing, W/m ²	Backward Differencing, W/m ²
I_{bn}	1.13	-1.10	1.23	-1.31
$I_{h,d}$	1.37	-1.28	1.50	-1.59
ρ	0.357	-0.357	0.566	-0.566
ϕ_b	-0.499	0.500	-0.291	0.303
$I_{bn} \times I_{h,d}$	-0.05596	-0.0831	0.0663	0.0531
$I_{bn} \times \rho$	0.00155	0.00158	0.00308	0.00310
$I_{bn} \times \phi_b$	-0.00464	-0.00464	-0.0027	-0.00274
$I_{h,d} \times \rho$	0.00352	0.00380	0.00514	0.00516
$I_{h,d} \times \phi_b$	-0.00267	-0.00264	-0.00094	-0.000907
$\rho \times \phi_b$	No Interactions	No Interactions	No Interactions	No Interaction
u	2.40	2.40	2.85	2.95

Table 4 Analysis of global vertical façade irradiance in W/m^2 ($\alpha_s > 0$) for Period 1.

Experiment	EnergyPlus Perez	DOE-2.1e Perez	TRNSYS-TUD Hay-Davies	TRNSYS-TUD Isotropic	TRNSYS-TUD Reindl	TRNSYS-TUD Perez	ESP-r Perez 1990	ESP-r Perez 1987	ESP-r Klucher	ESP-r Isotropic	ESP-r Muneer	
\bar{x}	176.1	169.7	177.2	165.1	157.8	170.9	169.8	188.2	192.8	174.8	171.9	191.4
s	223.8	211.8	218.6	205.1	190.1	209.4	211.1	218.2	220.5	196.9	192.5	226.3
x_{max}	856.8	817.8	820.4	801.2	743.2	810.4	796.4	804.7	806.7	743.5	728.8	915.7
x_{min}	0.2	0.3	0.0	0.4	0.9	0.4	0.3	0.2	0.1	0.3	0.3	0.2
\bar{D}	-	-6.4	1.1	-11.0	-18.3	-5.2	-6.3	1.9	6.6	-11.5	-14.3	5.1
$ \bar{D} $	-	13.7	10.5	18.0	26.2	15.7	11.7	13.3	14.7	24.6	27.8	14.1
D_{max}	-	103.5	67.1	108.0	138.9	90.4	73.3	87.7	86.7	139.1	157.7	205.5
D_{min}	-	0.0	0.0	0.0	0.0	0.0	0.0	0.0	0.0	0.0	0.0	0.0
D_{rms}	-	24.2	17.0	28.9	44.4	24.0	21.0	21.4	22.1	39.1	44.7	24.6
$D_{95\%}$	-	56.4	40.3	71.7	111.2	56.3	57.1	50.9	51.5	96.5	110.7	53.3
\overline{OU}	6.90	4.62	-	-	-	-	-	-	-	-	-	-
\overline{UR}	-	1.34	1.34	2.28	4.03	2.29	1.12	1.43	1.69	2.50	2.63	1.54
UR_{max}	-	12.42	20.41	20.41	129.05	20.41	10.20	11.22	12.09	17.04	17.04	13.48
UR_{min}	-	0.00	0.01	0.00	0.00	0.00	0.00	0.00	0.00	0.01	0.00	0.00
$ \bar{D} /\bar{x}$	-	7.8	5.9	10.2	14.9	8.9	6.7	6.7	6.7	14.8	16.7	7.2
\bar{D}/\bar{x}	-	-3.7	0.6	-6.2	-10.4	-3.0	-3.6	-2.7	-0.1	-11.3	-13.4	1.0

Table 5 Analysis of global vertical façade irradiance in W/m^2 ($\alpha_s > 0$) for Period 2.

Experiment	EnergyPlus Perez	DOE-2.1e Perez	TRNSYS-TUD Hay-Davies	TRNSYS-TUD Isotropic	TRNSYS-TUD Reindl	TRNSYS-TUD Perez	ESP-r Perez 1990	ESP-r Perez 1987	ESP-r Klucher	ESP-r Isotropic	ESP-r Muneer	
\bar{x}	194.5	208.5	210.5	199.7	191.6	207.7	201.4	202.0	206.7	190.1	187.9	202.5
s	222.1	226.3	231.3	219.0	201.5	224.1	225.2	222.4	223.8	201.3	197.3	224.2
x_{max}	797.1	796.3	828.5	807.8	741.4	820.2	801.7	794.6	799.5	730.4	720.2	801.1
x_{min}	0.3	0.3	0.0	0.4	0.4	0.4	0.3	0.2	0.2	0.3	0.3	0.2
\bar{D}	-	14.0	16.0	5.2	-2.9	13.2	6.9	7.5	12.2	-4.4	-6.6	8.0
$ \bar{D} $	-	19.4	17.6	16.2	25.0	19.0	12.7	14.6	17.2	23.4	26.4	15.4
D_{max}	-	104.0	77.3	59.5	122.6	67.2	63.5	81.3	86.7	113.0	134.9	86.9
D_{min}	-	0.0	0.1	0.1	0.1	0.1	0.0	0.0	0.0	0.0	0.0	0.0
D_{rms}	-	29.2	26.3	20.9	35.2	24.5	19.2	22.2	24.5	33.6	38.8	24.0
$D_{95\%}$	-	70.1	62.4	42.6	81.7	51.1	46.3	50.9	58.0	79.9	93.2	55.6
\overline{OU}	7.62	5.62	-	-	-	-	-	-	-	-	-	-
\overline{UR}	-	2.11	2.12	2.66	3.06	2.99	1.41	1.61	2.00	2.60	2.73	1.64
UR_{max}	-	12.83	21.70	20.62	20.63	21.41	11.21	9.70	11.24	14.94	14.94	13.48
UR_{min}	-	0.00	0.02	0.01	0.03	0.01	0.01	0.00	0.00	0.01	0.01	0.00
$ \bar{D} /\bar{x}$	-	10.0	9.1	8.3	12.9	9.8	6.5	7.5	8.8	12.0	13.6	7.9
\bar{D}/\bar{x}	-	7.2	8.2	2.7	-1.5	6.8	3.5	3.9	6.3	-2.3	-3.4	4.1

Table 6 Analysis of global vertical façade irradiance in W/m^2 ($\alpha_s > 0$) for both periods.

Experiment	EnergyPlus Perez	DOE-2.1e Perez	TRNSYS-TUD Hay-Davies	TRNSYS-TUD Isotropic	TRNSYS-TUD Reindl	TRNSYS-TUD Perez	ESP-r Perez 1990	ESP-r Perez 1987	ESP-r Klucher	ESP-r Isotropic	ESP-r Muneer	
\bar{x}	186.2	191.0	195.5	184.1	176.3	191.1	187.1	188.2	192.8	174.8	171.9	191.4
s	222.9	220.6	226.1	213.4	197.0	218.2	219.4	218.2	220.5	196.9	192.5	226.3
x_{max}	856.8	817.8	828.5	807.8	743.2	820.2	801.7	804.7	806.7	743.5	728.8	915.7
x_{min}	0.2	0.3	0.0	0.4	0.4	0.4	0.3	0.2	0.1	0.3	0.3	0.2
\bar{D}	-	4.8	9.3	-2.1	-9.9	4.9	0.9	1.9	6.6	-11.5	-14.3	5.1
$ \bar{D} $	-	16.8	14.4	17.0	25.6	17.5	12.2	13.3	14.7	24.6	27.8	14.1
D_{max}	-	104.0	77.3	108.0	138.9	90.4	73.3	87.7	86.7	139.1	157.7	205.5
D_{min}	-	0.0	0.0	0.0	0.0	0.0	0.0	0.0	0.0	0.0	0.0	0.0
D_{rms}	-	27.1	22.6	24.8	39.6	24.3	20.0	21.4	22.1	39.1	44.7	24.6
$D_{95\%}$	-	65.7	55.1	54.9	99.4	54.2	48.7	50.9	51.5	96.5	110.7	53.3
\overline{OU}	7.30	4.46	-	-	-	-	-	-	-	-	-	-
\overline{UR}	-	1.91	1.90	2.57	3.61	2.77	1.38	1.43	1.69	2.50	2.63	1.54
UR_{max}	-	17.62	29.31	28.31	129.05	29.39	15.38	11.22	12.09	17.04	17.04	13.48
UR_{min}	-	0.00	0.01	0.00	0.00	0.00	0.00	0.00	0.00	0.01	0.00	0.00
$ \bar{D} /\bar{x}$	-	9.0	7.7	9.1	13.7	9.4	6.6	7.2	7.9	13.2	14.9	7.6
\bar{D}/\bar{x}	-	2.6	5.0	-1.1	-5.3	2.6	0.5	1.0	3.5	-6.2	-7.7	2.8



Figure 1 Test cells with pyranometers visible in the central part of the picture and green artificial turf installed in front of the test cell.

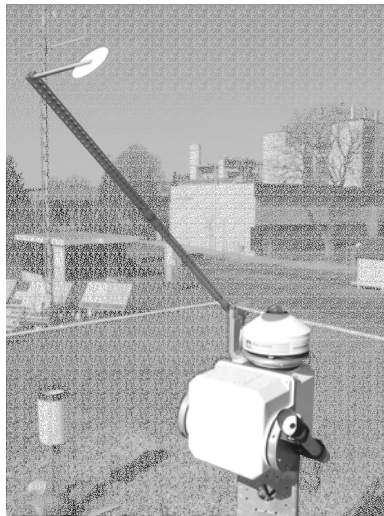


Figure 2 Pyrheliometer for measuring direct-normal and shaded pyranometer for measuring diffuse horizontal solar irradiance are positioned on the roof of the facility.

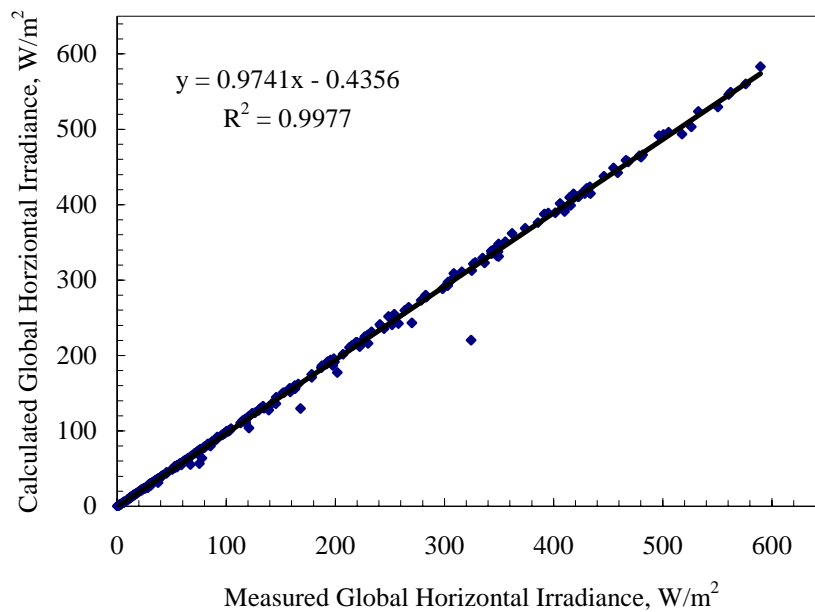


Figure 3a Measured and calculated global horizontal irradiance for Period 1.

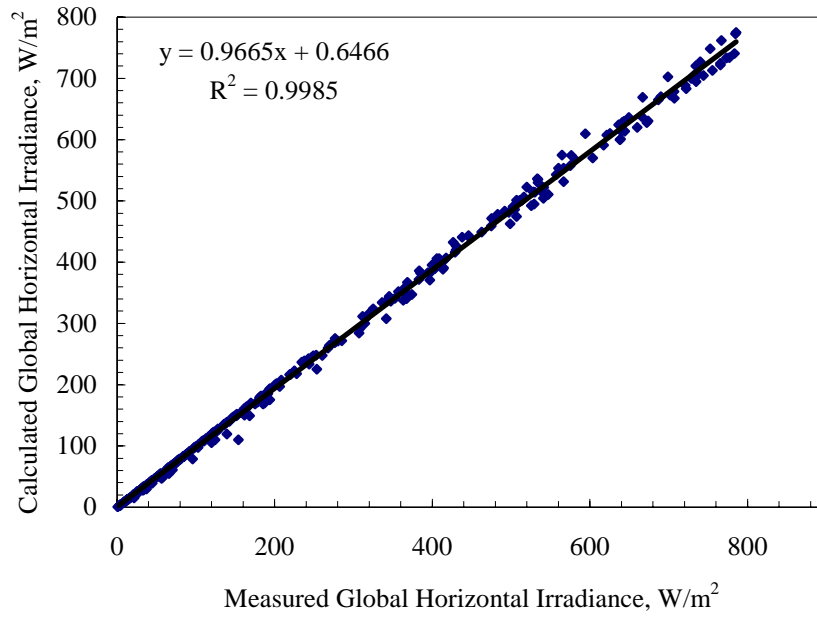


Figure 3b Measured and calculated global horizontal irradiance for Period 2.

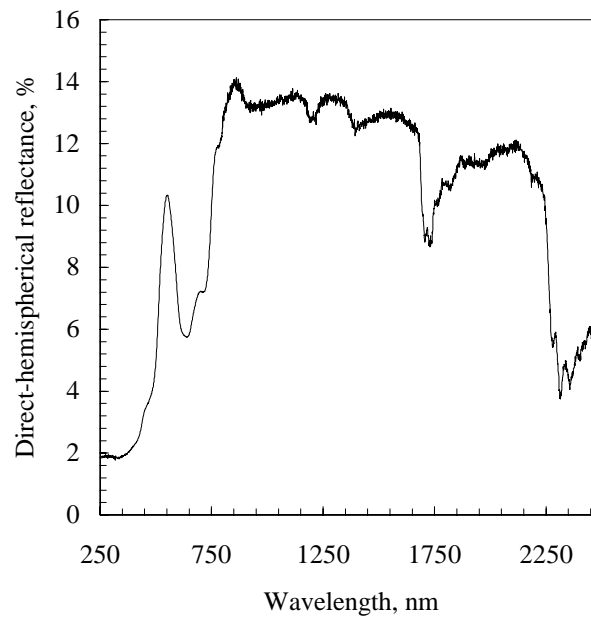


Figure 4 Directional-hemispherical reflectance of the artificial turf.

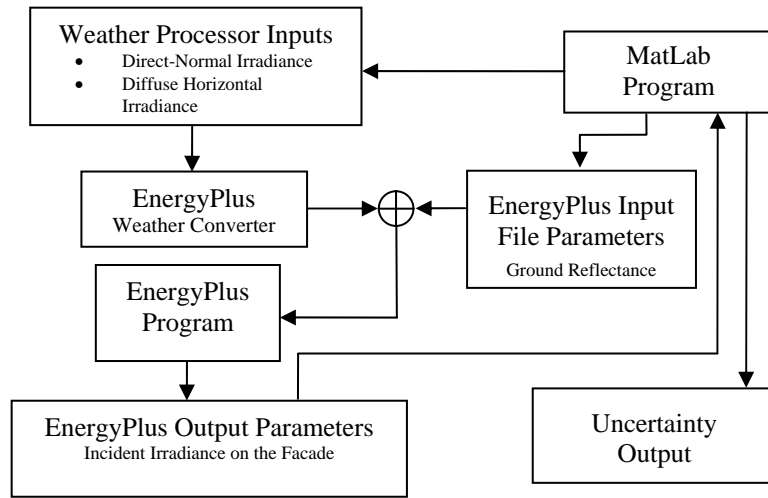


Figure 5 Flowchart for the sensitivity studies.

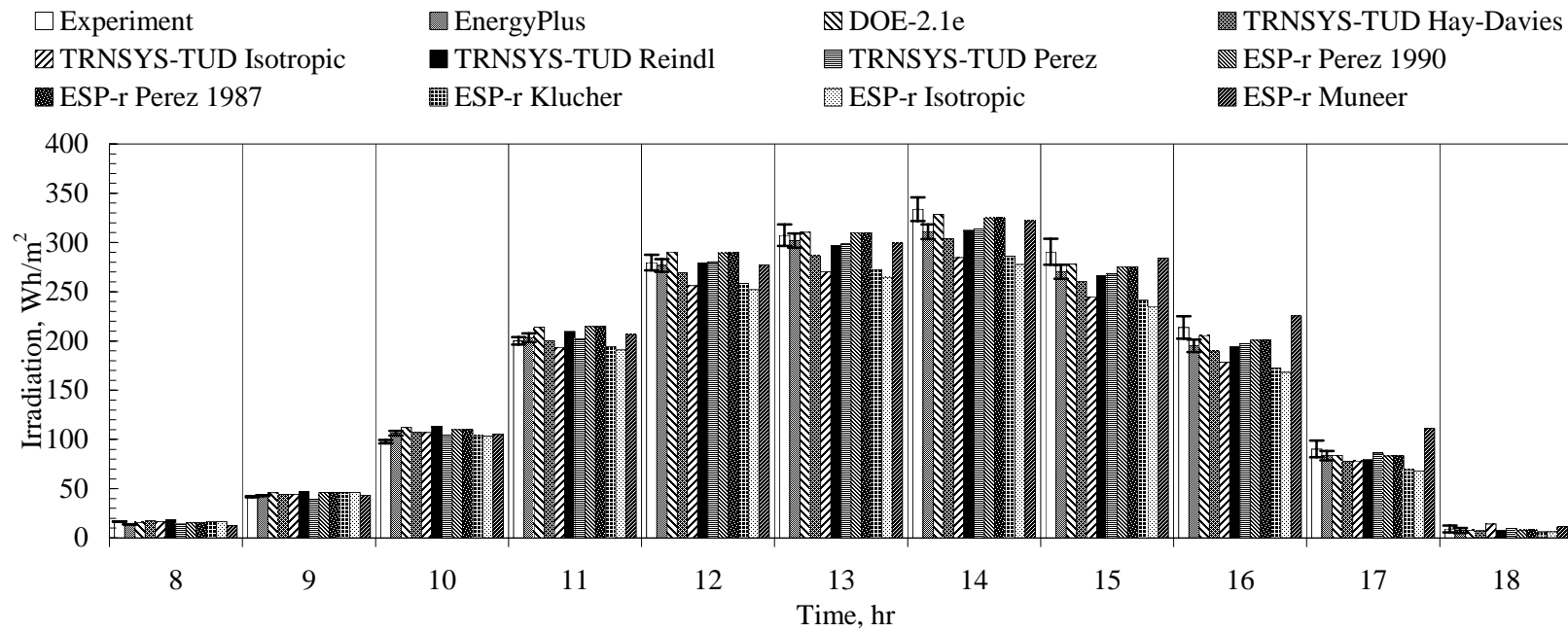


Figure 6 Average hourly irradiation comparisons for the vertical façade for Period 1.

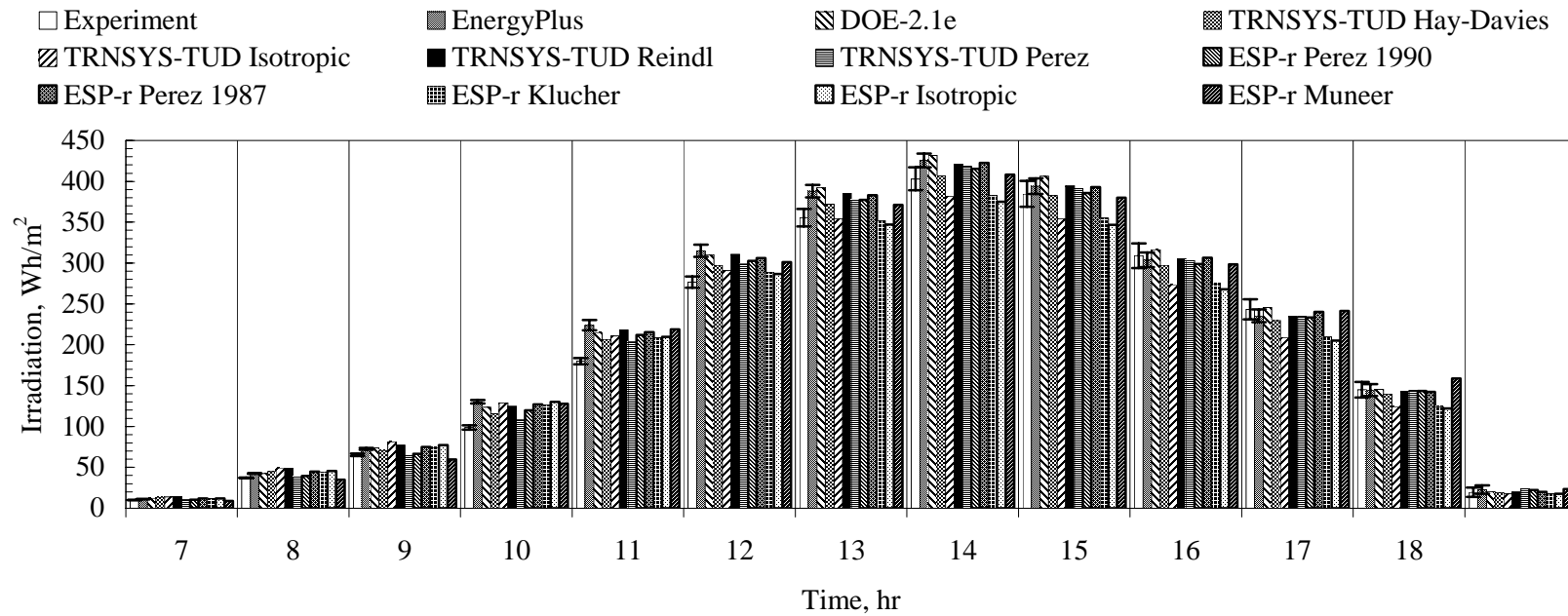


Figure 7 Average hourly irradiation comparisons for the vertical façade for Period 2.

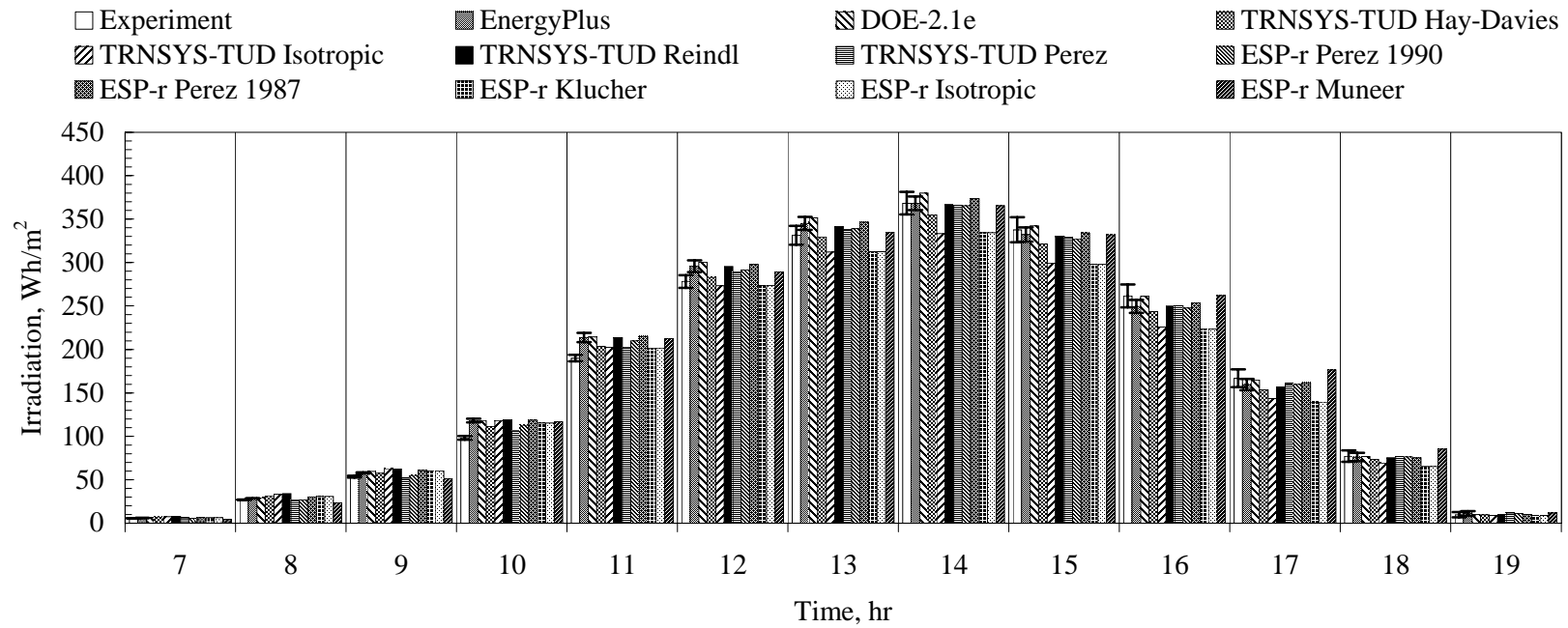


Figure 8 Average hourly irradiation comparisons for the vertical façade combining both periods.